Measuring the Berry phase in a superconducting phase qubit by a shortcut to adiabaticity

Zhenxing Zhang, Tenghui Wang, Liang Xiang, Jiadong Yao, Jianlan Wu, and Yi Yin

Phys. Rev. A **95**, 042345 — Published 28 April 2017

DOI: 10.1103/PhysRevA.95.042345

Measuring the Berry Phase in a Superconducting Phase Qubit by a Shortcut to Adiabaticity

Zhenxing Zhang,[1] Tenghui Wang,[1] Liang Xiang,[1] Jiadong Yao,[1] Jianlan Wu,[1] and Yi Yin[1,2,*]

[1] *Department of Physics, Zhejiang University, Hangzhou 310027, China*

[2] *Collaborative Innovation Center of Advanced Microstructures, Nanjing 210093, China*

Abstract

With a counter-diabatic field supplemented to the reference control field, the 'shortcut to adiabaticiy' (STA) protocol is implemented in a superconducting phase qubit. The Berry phase measured in a short time scale is in good agreement with the theoretical result acquired from an adiabatic loop. The trajectory of a qubit vector is extracted, verifying the Berry phase alternatively by the integrated solid angle. The classical noise is introduced to the amplitude or phase of the total control field. The mean of the Berry phase measured under either noise is almost equal to that without noise, while the variance under the amplitude noise can be described by an analytical expression.

* yiyin@zju.edu.cn

I. INTRODUCTION

In quantum mechanics, a geometric phase is acquired as a quantum state propagates on a curved surface and this interesting phenomenon is observed in many quantum systems ranging from microscopic particles to condensed matter materials [1–5]. The precise control and measurement of the geometric phase lead to geometric phase gates in quantum computation [6–10]. A typical example to understand the geometric phase is a spin-1/2 particle subject to a slowly-varying magnetic field which undergoes a closed path in the parameter space. In response to the changing field, the spin remains in an instantaneous eigenstate and follows a cyclic path in the Bloch sphere. The geometric phase, termed the Berry phase [1], is acquired by the spin state when the spin vector returns to its initial position. The Berry phase in such an adiabatic process is independent of the speed of the field's evolution if the adiabatic condition is satisfied.

In practice, a quantum manipulation is often performed in a short time scale to avoid dissipation induced errors, incompatible with the presumption of the adiabatic process. The advance of large-scale quantum devices requires fast operations to improve efficiency of information processing [11]. Various procedures have thus been proposed for the realization of a fast 'adiabatic' process [12–18]. One general strategy is to apply a 'shortcut to adiabaticity' (STA) where an additional Hamiltonian is employed to cancel the non-adiabatic contribution in a fast evolution [12–16]. For a given reference Hamiltonian $H_0(t)$, the counter-diabatic Hamiltonian $H_{\rm cd}(t)$ is formally written as [13]

$$H_{\rm cd}(t) = i\hbar \sum_n \left[\, |\partial_t n(t)\rangle\langle n(t)| - \langle n(t)|\partial_t n(t)\rangle \, |n(t)\rangle\langle n(t)| \, \right], \tag{1}$$

where $|n(t)\rangle$ is an instantaneous eigenstate of $H_0(t)$. For each eigenstate $|n(t)\rangle$, $H_{\rm cd}(t)$ suppresses its non-adiabatic transition to other eigenstates. The quantum system driven by the total Hamiltonian $H_{\rm tot}(t) = H_0(t) + H_{\rm cd}(t)$ can evolve fast but remain in the state $|n(t)\rangle$. Regardless of the evolution of $H_{\rm tot}(t)$, the system state evolves along a closed path with respect to $H_0(t)$ and acquires the associated Berry phase [19, 20].

The STA protocol has been implemented in atomic, molecular and optical systems for the state preparation, population transfer and optimal control [16, 21, 22]. Compared with these microscopic systems, a superconducting circuit is fabricated on chips with lithographic scalability. The superconducting qubit is realized based on nonlinear quantized energy levels

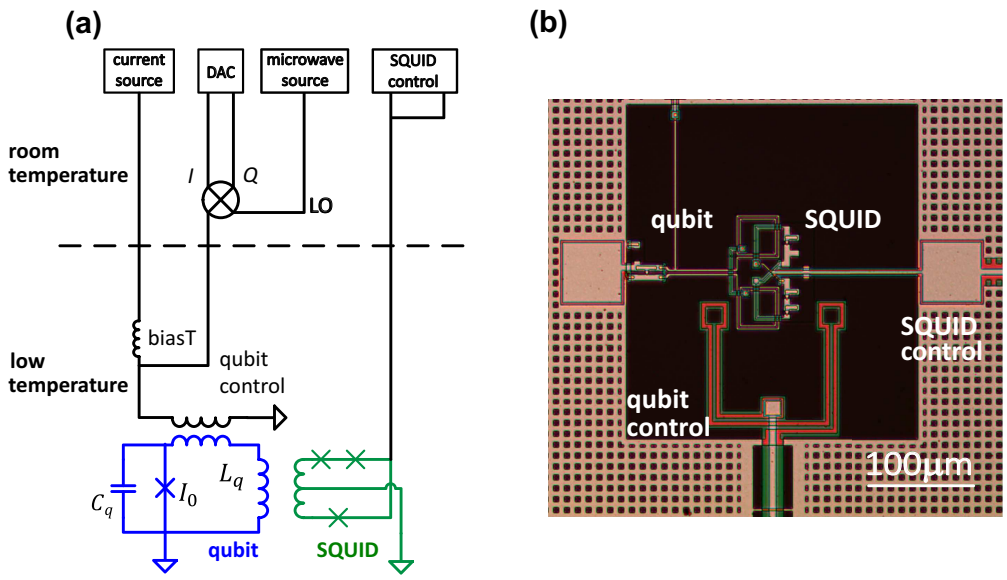

FIG. 1. (a) Schematic diagram of our experimental setup including the room-temperature control and the low-temperature phase qubit. (b) The optical micrograph of the phase qubit.

of the circuit. Sophisticated microwave techniques allow a reliable generation of the counter-diabatic Hamiltonian in superconducting qubits. In this paper, we focus on the realization of the STA protocol in a superconducting phase qubit [23, 24]. We achieve the Berry phase measurement with the STA protocol and study the influence of external field fluctuations, which extends previous studies of the Berry phase in a Cooper pair pump [25] and in an adiabatically-steered superconducting qubit [26, 27] .

II. EXPERIMENTAL SETUP

Figure 1(a) displays a schematic diagram of our experimental setup, including a phase qubit and external control lines [23]. The control signals are synthesized at room temperature, and then sent down to the low-temperature stage to manipulate and measure the qubit state. The phase qubit is mounted in a sample box and cooled in a dilution refrigerator whose base temperature is ~ 10 mK. As shown by the optical micrograph in Fig. 1(b), the main components are a qubit, a superconducting quantum interference device (SQUID) and their control lines. The circuit of a superconducting phase qubit is a nonlinear resonator comprised of a Josephson junction (with a critical current $I_0 = 2\ \mu$A), a loop inductance ($L_{\rm q}$ = 720 pH) and a capacitor ($C_{\rm q} = 1$ pF) [23, 24]. The flux currect biases this resonator in an

anharmonic cubic potential, and the lowest two energy levels of the nonlinear resonator are used as the ground ($|0\rangle$) and excited ($|1\rangle$) states of a qubit. In our experiment, the resonance frequency of the phase qubit is set at $\omega_{10}/2\pi = 5.7\,\mathrm{GHz}$, and the qubit dissipation is characterized by a relaxation time, $T_1 = 270\,\mathrm{ns}$, and a spin-echo decoherence time, $T_2^{\mathrm{echo}} = 450\,\mathrm{ns}$. The microwave drive signal is produced by mixing two low-frequency quadratures (I and Q) with the local oscillator (LO) signal (drive frequency ω_{d}), and provides a fast and reliable control of the qubit state.

For our phase qubit, it is difficult to perform an adiabatic operation [26, 27], but feasible to implement a fast STA protocol. With the qubit modelled as a spin-1/2 particle, we also treat the microwave signal as an effective external magnetic field. In the rotating frame of the external field, the Hamiltonian is expressed as $H(t) = \hbar \boldsymbol{B}(t) \cdot \boldsymbol{\sigma}/2$ after the rotating wave approximation. Here $\boldsymbol{\sigma} = (\sigma_x, \sigma_y, \sigma_z)$ is the vector of Pauli operators and $\boldsymbol{B}(t)$ is the effective magnetic field expressed in the unit of angular frequency. Throughout this paper, our experiment will be described and discussed in the rotating frame. At the end of a quantum operation, the qubit state is projected to either the ground ($|0\rangle$) or excited ($|1\rangle$) state for the readout measurement [23]. As the ground and excited states induce different fluxes in the qubit loop, the SQUID can detect the probability of the two states through the SQUID control line. Furthermore, the quantum state tomography (QST) technique is applied in the readout to extract the density matrix of the final qubit state.

III. EXPERIMENTAL MEASUREMENT OF THE BERRY PHASE WITH THE STA PROTOCOL

In an adiabatic process, the Berry phase can be measured with a spin-echo scheme [26–28]. In our STA experiment, the reference Hamiltonian, $H_0(t) = \hbar \boldsymbol{B}_0(t) \cdot \boldsymbol{\sigma}/2$, is used to construct the spin-echo trajectory in a short time scale. As shown in Fig. 2(a), the reference magnetic field $\boldsymbol{B}_0(t)$ evolves as follows. A $\pi/2$-pulse is applied to the ground-state qubit, preparing an initial superposition state at $(|0\rangle + |1\rangle)/\sqrt{2}$. After the initialization, the first sequence of the field, $\boldsymbol{B}_{\mathrm{ramp},0}(t_1) = (\Delta_0 \tan\theta(t_1), 0, \Delta_0)$ with $0 < t_1 < T_{\mathrm{ramp}}$, ramps up its x-component by $\theta(t_1) = \theta_0 t_1/T_{\mathrm{ramp}}$. The ramping time is fixed at $T_{\mathrm{ramp}} = 10$ ns, while $\Delta_0 = \omega_{\mathrm{d}} - \omega_{10}$ is the detuning between the microwave drive frequency ω_{d} and the qubit resonance frequency ω_{10}. We set $\Delta_0/2\pi = 7$ MHz to reduce the influence of higher excited states. The second sequence

builds a rotating field, $\boldsymbol{B}_{\mathrm{rot},0}(t_2) = (\Omega_0 \cos\phi(t_2), \Omega_0 \sin\phi(t_2), \Delta_0)$ with $0 < t_2 < T_{\mathrm{rot}}$. The drive amplitude is $\Omega_0 = \Delta_0 \tan\theta_0$, while the rotation is operated under a constant speed $\omega_0 = 2\pi/T_{\mathrm{rot}}$ along either the counterclockwise ($\mathcal{C}_+$) or clockwise ($\mathcal{C}_-$) direction. The time-dependent phase of the effective field is given by $\phi(t_2) = \pm\omega_0 t_2$. In our experiment, the pre-designed polar angle θ_0 and the rotation time T_{rot} are varied as control parameters. To further reduce the influence of higher excited states, a reversed ramping-down field, $\boldsymbol{B}_{\mathrm{ramp},0}(T_{\mathrm{ramp}} - t_3)$ with $0 < t_3 < T_{\mathrm{ramp}}$, is subsequently used to finish the first (dephasing) part of the spin-echo scheme [29]. A refocusing π-pulse is then applied to invert the qubit states. During the second (rephasing) part of our spin-echo scheme, the three sequences in the first part are reversed, as shown in Fig. 2(a). Based on the cyclic rotations in the dephasing and rephasing parts, the symbols of $\mathcal{C}_{+-}$ and $\mathcal{C}_{-+}$ represent two different types of spin-echo procedures.

To fulfill the STA protocol, the counter-diabatic Hamiltonian, $H_{\mathrm{cd}}(t) = \hbar\boldsymbol{B}_{\mathrm{cd}}(t)\cdot\boldsymbol{\sigma}/2$, is calculated by Eq. (1). For each ramping or rotating step, the counter-diabatic magnetic field is given by $\boldsymbol{B}_{\mathrm{cd}}(t) = \boldsymbol{B}_0(t) \times \dot{\boldsymbol{B}}_0(t)/|\boldsymbol{B}_0(t)|^2$, which is perpendicular to the reference magnetic field (see Appendix A). In particular, the counter-diabatic ramping field is written as $\boldsymbol{B}_{\mathrm{ramp,cd}}(t) = (0, \pm\theta_0/T_{\mathrm{ramp}}, 0)$, where the $\pm$ signs correspond to the ramping-up and ramping-down steps, respectively. The counter-diabatic rotating field is written as $\boldsymbol{B}_{\mathrm{rot,cd}}(t) = (\Omega_{\mathrm{cd}} \cos\phi(t), \Omega_{\mathrm{cd}} \sin\phi(t), \Delta_{\mathrm{cd}})$, where the signs of $\Omega_{\mathrm{cd}} = \mp\omega_0 \sin\theta_0 \cos\theta_0$ and $\Delta_{\mathrm{cd}} = \pm\omega_0 \sin^2\theta_0$ refer to the $\mathcal{C}_+$ and $\mathcal{C}_-$ rotations, respectively. The total magnetic field is obtained as $\boldsymbol{B}_{\mathrm{tot}}(t) = \boldsymbol{B}_0(t) + \boldsymbol{B}_{\mathrm{cd}}(t)$, an example of which is shown in Fig. 2(a).

In the STA protocol, the qubit is designed to follow the path of $\boldsymbol{B}_0(t)$ when driven by the total Hamiltonian $H_{\mathrm{tot}}(t) = \hbar\boldsymbol{B}_{\mathrm{tot}}(t)\cdot\boldsymbol{\sigma}/2$. Initially, the $|0\rangle$ and $|1\rangle$ states are the instantaneous spin-up ($|s_\uparrow(t)\rangle$) and spin-down ($|s_\downarrow(t)\rangle$) eigenstates of the reference Hamiltonian, respectively. In an ideal adiabatic scenario, the Bloch vector of the $|s_\uparrow(t)\rangle$ state always points to the same direction of $\boldsymbol{B}_0(t)$, while the opposite occurs for the $|s_\downarrow(t)\rangle$ state. The ramping sequences only produce a dynamic phase, while both the dynamic and Berry phases are acquired during circular rotations. For the $|s_\uparrow(t)\rangle$ state, the Berry phase accumulated in one cycle is given by $\gamma_\uparrow = \mp\mathcal{S}/2$, where $\mathcal{S} = 2\pi(1 - \cos\theta_0)$ is the solid angle of the cone subtended by the cyclic path at the origin and the $\mp$ signs refer to the $\mathcal{C}_+$ or $\mathcal{C}_-$ paths, respectively. Since the $|s_\downarrow(t)\rangle$ state follows the opposite path of the $|s_\uparrow(t)\rangle$ state, its accumulated Berry phase is opposite, i.e., $\gamma_\downarrow = \pm\mathcal{S}/2$. After the refocusing π pulse, the phases

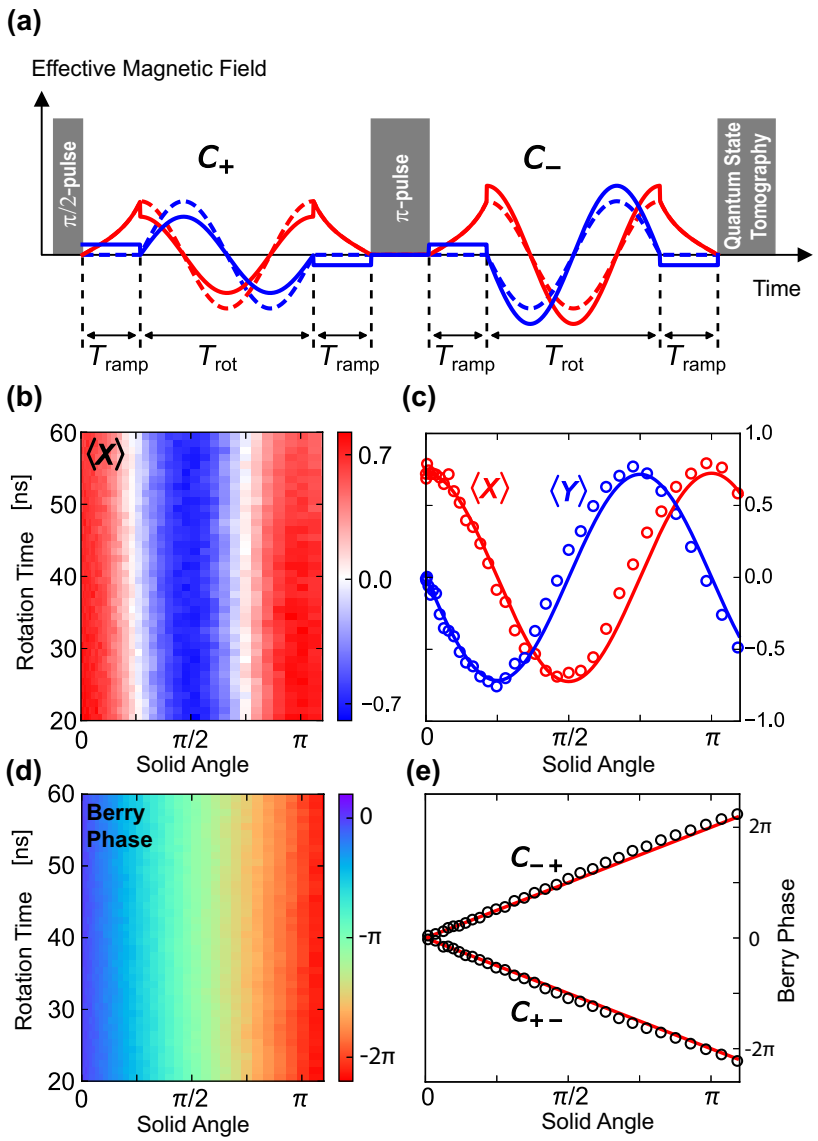

FIG. 2. The STA experiment of measuring the Berry phase with a $\mathcal{C}_{+-}$ spin-echo procedure. (a) The schematic diagram of the effective magnetic field in the x-y plane. The dashed and solid lines are the reference and total control fields, while the red and blue colors refer to their x- and y-components. (b) The measurement of the x-projection of the final qubit state versus the solid angle $\mathcal{S}$ and the rotation time $T_{\rm rot}$. (c) With $T_{\rm rot} = 30$ ns, the x-, y-projections of the final qubit state (red and blue circles) are compared with the theoretical prediction (red and blue lines). (d) The measurement of the Berry phase versus $\mathcal{S}$ and $T_{\rm rot}$. (e) With $T_{\rm rot} = 30$ ns, the extracted Berry phase (circles) is compared with the theoretical prediction (solid line). The comparison between the experimental measurement and the theoretical prediction in the $\mathcal{C}_{-+}$ procedure is also presented.

associated with the $|s_\uparrow(t)\rangle$ and $|s_\downarrow(t)\rangle$ states are swapped. For each instantaneous eigenstate, the dynamic phase is cancelled in the rephasing part, while the Berry phase is doubled due to a reversed rotating direction. At the echo time, the $|s_\uparrow(t)\rangle$ and $|s_\downarrow(t)\rangle$ states return to the two poles of the Bloch sphere, and the final qubit state is written as $(e^{-i\gamma/2}\,|0\rangle + e^{i\gamma/2}|1\rangle)/\sqrt{2}$ with a global phase excluded. The total relative Berry phase after two circular rotations is theoretically given by $\gamma = \mp 2\mathcal{S}$ for the $\mathcal{C}_{+-}$ or $\mathcal{C}_{-+}$ procedures, respectively.

In our experiment, the total field $\boldsymbol{B}_{\rm tot}(t)$ is realized by the microwave control signal, and the qubit is driven in the spin-echo scheme as above. To measure the Berry phase γ, we apply the QST to extract the density matrix ρ of the final state [24]. The x- and y-projections of the qubit vector are given by $\langle x\rangle = {\rm Tr}\{\sigma_x\rho\}$ and $\langle y\rangle = {\rm Tr}\{\sigma_y\rho\}$. The two-dimensional (2D) diagram in Fig. 2(b) presents the experimental measurement of $\langle x\rangle$ with the change of the rotation time $T_{\rm rot}$ and the pre-designed solid angle $\mathcal{S}$ (through the change of θ_0) in the $\mathcal{C}_{+-}$ procedure. The rotation time, 20 ns $\leq T_{\rm rot} \leq$ 60 ns, in our experiment is much shorter than the necessary time ($T_{\rm rot} \gtrsim 1$ μs) of an adiabatic operation [26] . We observe that $\langle x\rangle$ oscillates with $\mathcal{S}$ and varies slowly with $T_{\rm rot}$; the same conclusion is applied to $\langle y\rangle$ (not shown). From the results of $T_{\rm rot} = 30$ ns in Fig. 2(c), these two components are consistent with the theoretical prediction of $\langle x\rangle = r\cos\gamma$ and $\langle y\rangle = r\sin\gamma$ with $\gamma = -2\mathcal{S}$. Here $r = 0.72$ is an adjusted fitting parameter due to dissipation. On the other hand, these two oscillations are nearly undamped with $\mathcal{S}$, indicating a weak geometric dephasing [26]. For each final density matrix, the Berry phase γ is estimated using $\arctan[\langle y\rangle/\langle x\rangle]$. In the $\mathcal{C}_{+-}$ procedure, the Berry phase with $\theta_0 < \pi/3$ (or $\mathcal{S} < \pi$) is assigned in the range of $(-2\pi, 0)$ after considering the signs of $\langle x\rangle$ and $\langle y\rangle$. With $\pi/3 < \theta_0 < \pi/2$ (or $\pi < \mathcal{S} < 2\pi$), an extra -2π is included to assign γ in the range of $(-4\pi, -2\pi)$. An opposite range is specified for γ in the $\mathcal{C}_{-+}$ procedure. Figure 2(d) presents the measurement of γ for the $\mathcal{C}_{+-}$ procedure. From the result of $T_{\rm rot} = 30$ ns in Fig. 2(e), the linear relation, $\gamma = -k\mathcal{S}$ ($k = 2.04 \pm 0.02$), is extracted, in good agreement with the theoretical prediction of $\gamma = -2\mathcal{S}$. The same relation with an opposite sign, $\gamma = k'\mathcal{S}$ ($k' = 2.06 \pm 0.02$), is extracted for the $\mathcal{C}_{-+}$ procedure. The two slopes, k and k', are almost unchanged with the increase of the rotation time $T_{\rm rot}$. Our experiment thus demonstrates that the Berry phase of a cyclic adiabatic path can be successfully measured in the superconducting phase qubit following the fast STA protocol.

To further illustrate the accumulation of the Berry phase, we modify the external microwave signal and inspect the trajectory of the $|s_\uparrow(t)\rangle$ state in the STA protocol. Without

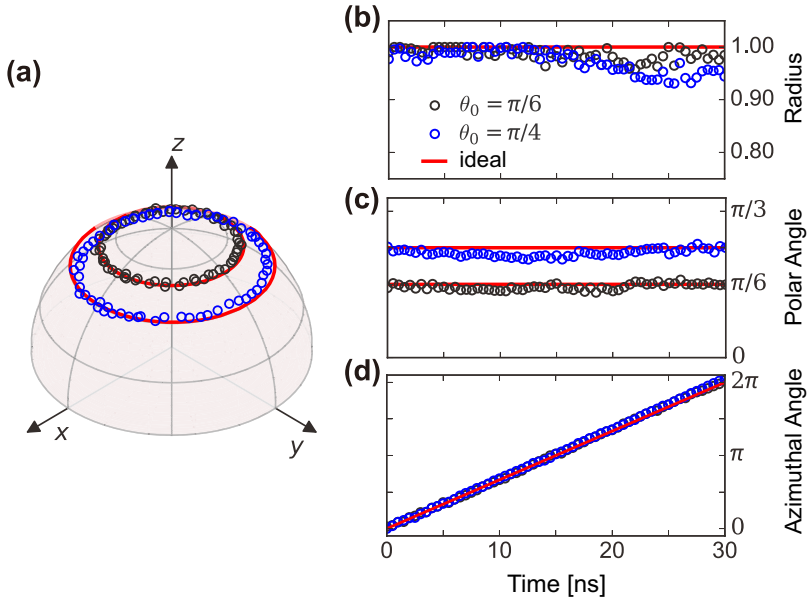

FIG. 3. In the STA procedure, the evolution of the $|s_{\uparrow}(t)\rangle$ state subject to a $\mathcal{C}_+$-rotating field with $T_{\rm rot} = 30$ ns. (a) The trajectory of the qubit vector in the Bloch sphere. In the spherical coordinate system of the qubit vector, the time evolutions of radius, polar and azimuthal angles are plotted in (b), (c) and (d), respectively. In (a)-(d), the black and blue circles are the experimental results of $\theta_0 = \pi/6$ and $\pi/4$, respectively. The associated solid lines are the results of an ideal evolution.

the excitation of the $\pi/2$-pulse, the ground-state qubit (or the $|s_{\uparrow}(t)\rangle$ state) is driven by the ramping-up field $\boldsymbol{B}_{\rm ramp,tot}(t_1)$ and the subsequent $\mathcal{C}_+$-rotating field $\boldsymbol{B}_{\rm rot,tot}(t_2)$ with $T_{\rm rot} = 30$ ns. We measure the density matrix of the qubit by interrupting the rotation and performing the QST every 0.5 ns. Figure 3 presents the time evolution of the qubit vector during the rotation period for two pre-designed polar angles, $\theta_0 = \pi/6$ and $\pi/4$, in the parameter space. As shown in Figs. 3(c) and 3(d), the polar angles of both qubit vectors vary weakly with time (around the given value of θ_0), and their azimuthal angles increase almost linearly with the time as $\phi(t_2) = \omega_0 t_2$. The time evolution of the radii in Fig. 3(b) shows that the two qubit vectors are initially on the surface of the Bloch sphere and slightly shrink due to dissipation. Our experiment confirms that the $|s_{\uparrow}(t)\rangle$ state follows the same direction of $\boldsymbol{B}_{\rm rot,0}(t_2)$ and takes a circular path along the latitude of $\pi/2 - \theta_0$ in the northern hemisphere. An integration, $\mathcal{S} = \int [1 - \cos\theta(t_2)] d\phi(t_2)$, further allows us to estimate the actual solid angles enclosed by the circular path. The approximate integration results, $\mathcal{S}(\theta_0 = \pi/6) = 0.788$ and $\mathcal{S}(\theta_0 = \pi/4) = 1.72$, are roughly close to their theoretical values of $\mathcal{S} = 2\pi(1 - \cos\theta_0)$

in an ideal adiabatic scenario, also consistent with the measurement of the Berry phase in Fig. 2.

IV. NOISE EFFECT OF THE BERRY PHASE MEASUREMENT

In a previous experiment of a superconducting transmon qubit with the adiabatic protocol, the stability of the Berry phase was studied under the influence of slowly-varying noises [27, 30]. Similarly, we introduce an artificial fluctuation $\delta\boldsymbol{B}_{\rm rot}(t)$ to the rotation field $\boldsymbol{B}_{\rm rot,tot}(t)$. Two independent stochastic noises, $\delta\Omega(t)$ and $\delta\phi(t)$, are assigned to the drive amplitude and phase of the effective magnetic field in the x-y plane, respectively. Both noises are assumed to follow the Ornstein-Uhlenbeck (O-U) process. The amplitude noise satisfies $\langle\delta\Omega(t)\rangle = 0$ and $\langle\delta\Omega(t)\delta\Omega(0)\rangle = c_\Omega^2\Omega_{\rm tot}^2\exp(-\Gamma t)$ with $\Omega_{\rm tot} = \Omega_0 + \Omega_{\rm cd}$, while the phase noise satisfies $\langle\delta\phi(t)\rangle = 0$ and $\langle\delta\phi(t)\delta\phi(0)\rangle = c_\phi^2\exp(-\Gamma t)$. The dimensionless coefficients, c_Ω and c_ϕ, represent the reduced noise strengths. A small noise bandwidth, $\Gamma = 10$ MHz, is chosen so that noises are correlated through the operation time. In our experiment, we investigate the influence of the amplitude noise $\delta\Omega(t)$ and the phase noise $\delta\phi(t)$ separately. With respect to each noise parameter (c_Ω and c_ϕ), the total 300 stochastic trajectories of $\delta\boldsymbol{B}_{\rm rot}(t)$ are generated. Since the relative dynamic phase between the $|s_\uparrow(t)\rangle$ and $|s_\downarrow(t)\rangle$ states cannot be cancelled by a noisy spin-echo sequence, we only assign a single rotating field, $\boldsymbol{B}_{\rm rot,tot}(t) + \delta\boldsymbol{B}_{\rm rot}(t)$, to measure the Berry phase accumulated in a single cycle. To reduce the influence of the intrinsic noise, the spin-echo scheme is still used, while the effective magnetic field is only applied in the second part following the π-pulse. An example of the noisy magnetic field with the $\mathcal{C}_+$ rotation is shown in Fig. 4(a). For each noisy sequence, we measure the final density matrix by the QST and unwrap the total accumulated phase, similar to the method in Fig. 2. The final relative Berry phase γ ($|s_\downarrow(t)\rangle$ relative to $|s_\uparrow(t)\rangle$) from one circular loop is then estimated from the total phase subtracted by a theoretical calculation of the dynamic phase (see Appendix B). This indirect approach could introduce a small error of the dynamic phase into the estimation of γ, which however does not affect the main conclusion of our experiment. After collecting data over 300 trajectories, we obtain the statistics of γ subject to the amplitude noise $\delta\Omega(t)$ or the phase noise $\delta\phi(t)$.

With a fixed rotation time, $T_{\rm rot} = 30$ ns, we first study the variation of the Berry phase under a given noise strength, $c_\Omega = 0.1$ or $c_\phi = 0.1$. For four pre-designed solid angles,

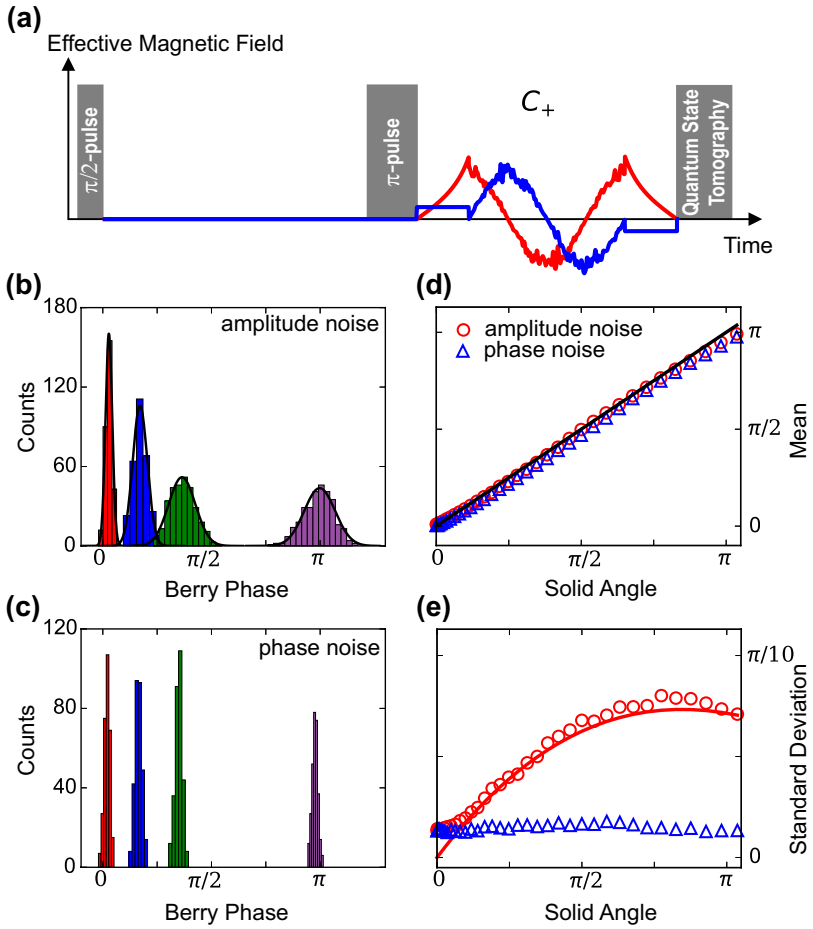

FIG. 4. The STA experiment of studying the noise influence on the measurement of the Berry phase. (a) The schematic diagram of the effective magnetic field with a noisy $\mathcal{C}_+$-rotation. The red and blue colors refer to the x- and y-components of the total control field. With $T_{\rm rot} = 30$ ns, the histograms of the Berry phase subject to 300 trajectories of the amplitude ($c_\Omega = 0.1$) and phase noises ($c_\phi = 0.1$) are plotted in (b) and (c), respectively. From the left to right in both (b) and (c), the four distributions refer to the results of $\mathcal{S} = \pi/40, 3\pi/16, 3\pi/8$, and π in the parameter space. In (b), the solid lines are the Gaussian fitting curves of the histograms. The mean value and standard deviation are shown in (d) and (e), where the circles and up-triangles refer to the experimental results of the amplitude and phase noises, respectively. In (d), the solid line is the result without noise. In (e), the solid line is the analytical prediction of Eq. (2).

$\mathcal{S} = \pi/40, 3\pi/16, 3\pi/8$, and π in the parameter space, the histograms of γ subject to the amplitude and phase noises are presented in Figs. 4(b) and 4(c), respectively. For the amplitude noise, each histogram is well fitted by a Gaussian distribution, $\exp[-(\gamma-\bar{\gamma}_\Omega)^2/2\sigma_\Omega^2]$, predicted by an analytical theory derived in Appendix B [30]. As verified in Fig. 4(d), the mean value of the Berry phase over various noise trajectories, $\bar{\gamma}_\Omega$, is very close to the result of $\gamma = \mathcal{S}$ from a single circular loop without noise. In the leading order of c_Ω, the standard deviation σ_Ω is analytically expressed as

$$\sigma_\Omega = 2\sqrt{2}c_\Omega \pi \sin^2\theta_0 \cos\theta_0 \frac{\sqrt{\Gamma T_{\rm rot} - 1 + e^{-\Gamma T_{\rm rot}}}}{\Gamma T_{\rm rot}}. \tag{2}$$

Figure 4(e) shows that the experimental measurement of σ_Ω agrees well with Eq. (2) over a broad range of $\mathcal{S}$. At small solid angles, a residue $\sim 0.02\pi$ is observed for σ_Ω, which may be attributed to the intrinsic noise of the qubit. Equation (2) indicates an upper deviation limit, $\sigma_\Omega \sim 2c_\Omega \pi \sin^2\theta_0 \cos\theta_0$, for the STA process. For the parameters $\Gamma T_{\rm rot} = 0.3$ and $c_\Omega = 0.1$ in our experiment, Fig. 4(e) demonstrates that the fluctuation of the Berry phase is still tolerable with $\sigma_\Omega < 0.1\pi$. As a comparison, the influence of the phase noise is much weaker than that of the amplitude noise, which can be identified by the narrow distributions of γ in Fig. 4(c). This behavior is due to the fact that the Berry phase depends on the geometry of the circular path instead of the rotating speed [30]. Accordingly, the mean $\bar{\gamma}_\phi$ is close to the result without noise [Fig. 4(d)] and the standard deviation σ_ϕ is consistently small, $\sigma_\phi \sim 0.02\pi$, over the whole range of the solid angle [Fig. 4(e)].

A coherence parameter, $\nu = |\langle \exp(i\gamma) \rangle|$, can alternatively quantify the fluctuation of the Berry phase [27]. For the amplitude noise ($c_\Omega = 0.1$) and phase noise ($c_\phi = 0.1$), the $\mathcal{S}$-dependencies of ν_Ω and ν_ϕ in Fig. 5(a) are consistent with the results of σ_Ω and σ_ϕ in Fig. 4(e). The effect of the phase noise is essentially negligible whereas the influence of the amplitude noise is well described by an analytical expression. Furthermore, we explore the change of the coherence parameter as the noise strength (c_Ω or c_ϕ) varies. For a fixed polar angle, $\theta_0 = \pi/3$ (or $\mathcal{S} = \pi$), Fig. 5(b) confirms the weak influence of the phase noise. As a comparison, ν_Ω can maintain a large value for $c_\Omega < 0.2$ while a major drop of ν_Ω occurs for $c_\Omega > 0.5$. In both Figs. 5(a) and 5(b), the results of ν_Ω can be well described by $\nu_\Omega = \exp(-\sigma_\Omega^2/2)$, where the analytical values of σ_Ω from Eq. (2) are used.

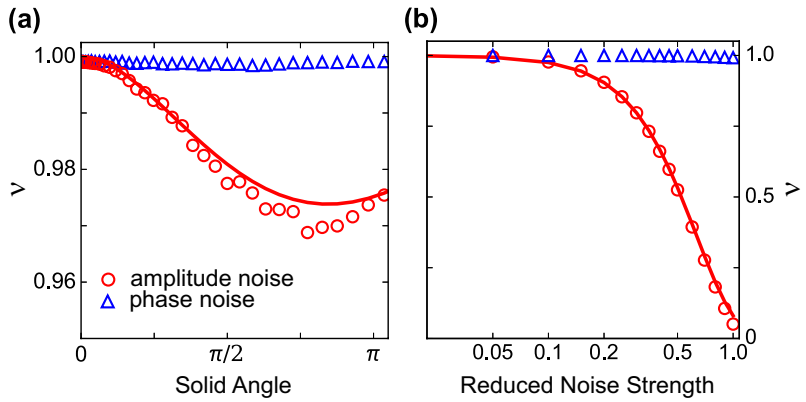

FIG. 5. The coherence parameter ν under two types of noises with the rotation time $T_{\rm rot} = 30$ ns. (a) The results of ν versus the solid angle $\mathcal{S}$ for the noise strengths of $c_\Omega = 0.1$ and $c_\phi = 0.1$. (b) The results of ν versus c_Ω and c_ϕ for $\mathcal{S} = \pi$. In both (a) and (b), the circles and up-triangles refer to the experimental results of the amplitude and phase noises, respectively. For the amplitude noise, the two solid lines are the results of $\nu_\Omega = \exp(-\sigma_\Omega^2/2)$ with σ_Ω calculated by Eq. (2).

V. SUMMARY

In summary, we have implemented the STA protocol in a superconducting phase qubit. In good agreement with the theoretical prediction, the Berry phase is successfully measured in a time (20 ns $\leq T_{\rm rot} \leq$ 60 ns) much shorter than that required by the adiabatic theorem ($T_{\rm rot} \gtrsim 1$ μs). The measurement of the Berry phase is almost independent of the operation time, which is a characteristic property of the STA protocol. The trajectory of a qubit state is verified, from which the solid angle enclosed by the path is calculated to understand the accumulation of the Berry phase. Classical fluctuations of the drive amplitude or phase are artificially introduced to the total control field. Our experiment shows that the mean value of the Berry phase is unchanged, while the standard deviation with the amplitude noise can be described by an analytical expression. To further understand the stability of the Berry phase, an extended study of quantum noise will be necessary in the future [31, 32]. The fast measurement of the Berry phase in this paper will hopefully encourage more applications of the STA protocol in superconducting qubit systems.

ACKNOWLEDGMENTS

This work is supported by the National Basic Research Program of China (2014CB921203, 2015CB921004), the National Natural Science Foundation of China (NSFC-11374260, NSFC-21173185), and the Fundamental Research Funds for the Central Universities in China. Devices were made at John Martinis's group using equipments of UC Santa Barbara Nanofabrication Facility, a part of the NSF-funded National Nanotechnology Infrastructure Network.

Appendix A: The Shortcut to Adiabaticity Protocol

In this Appendix, we provide a theoretical derivation of the STA protocol, which is slightly different from the original one in Ref. [13] but leads to the same result. For a general quantum system, we consider a non-degenerate time-dependent Hamiltonian $H_0(t) = \sum_n \varepsilon_n(t)|n(t)\rangle\langle n(t)|$, where $|n(t)\rangle$ is the n-th instantaneous eigenstate associated with the eigenenergy $\varepsilon_n(t)$. Each wavefunction can be linearly decomposed into $|\psi(t)\rangle = \sum_n a_n(t)|n(t)\rangle$ with $a_n(t)$ the time-dependent coefficient. Following the Schrodinger equation, the time evolution of $a_n(t)$ is given by

$$\hbar\dot{a}_n(t) = -i\left[\varepsilon_n(t) - i\hbar\langle n(t)|\partial_t n(t)\rangle\right] a_n(t) - \hbar\sum_{m(\neq n)}\langle n(t)|\partial_t m(t)\rangle a_m(t). \tag{A1}$$

In the adiabatic limit, the second term on the right hand side of Eq. (A1) vanishes and only a phase $\varphi_n(t)$ is accumulated with time, i.e., $a_n(t) = \exp[i\varphi_n(t)]a_n(0)$.

However, the influence from other eigenstates $|m(t)\rangle$ cannot be ignored if the time propagation of $H_0(t)$ is not slow enough. To achieve a fast 'adiabaticity', the STA protocol was proposed through the assistance of a counter-diabatic Hamiltonian $H_{\rm cd}(t)$. For the total Hamiltonian, $H_{\rm tot}(t) = H_0(t) + H_{\rm cd}(t)$, the wavefunction, $|\psi(t)\rangle = \sum_n a_n(t)|n(t)\rangle$, is still decomposed using the eigen basis set of the reference Hamiltonian $H_0(t)$. The time evolution of $a_n(t)$ is changed to be

$$\begin{aligned}\hbar\dot{a}_n(t) = &-i\left[\varepsilon_n(t) - i\hbar\langle n(t)|\partial_t n(t)\rangle\right] a_n(t) - i\langle n(t)|H_{\rm cd}(t)|n(t)\rangle a_n(t)\\ &-i\sum_{m(\neq n)}\left[-i\hbar\langle n(t)|\partial_t m(t)\rangle + \langle n(t)|H_{\rm cd}(t)|m(t)\rangle\right] a_m(t).\end{aligned} \tag{A2}$$

To recover the adiabatic time evolution, the counter-diabatic Hamiltonian is required to

satisfy

$$\begin{cases} \langle n(t)|H_{\rm cd}(t)|n(t)\rangle = 0 \\ \langle n(t)|H_{\rm cd}(t)|m(t)\rangle = i\hbar\langle n(t)|\partial_t m(t)\rangle \quad \text{for} \quad m \neq n \end{cases}. \tag{A3}$$

Since the indices, m and n, are arbitrary, the action of $H_{\rm cd}(t)$ applied to each $|n(t)\rangle$ must follow $H_{\rm cd}(t)|n(t)\rangle = i\hbar[|\partial_t n(t)\rangle - \langle n(t)|\partial_t n(t)\rangle|n(t)\rangle]$. The counter-diabatic Hamiltonian is thus given by

$$H_{\rm cd}(t) = i\hbar \sum_n \big[|\partial_t n(t)\rangle - \langle n(t)|\partial_t n(t)\rangle|n(t)\rangle\big]\langle n(t)|, \tag{A4}$$

which satisfies $\sum_{m,n} H^*_{0;m,n}(t)H_{{\rm cd};m,n}(t) = 0$. For a spin-1/2 particle with the reference Hamiltonian $H_0(t) = \hbar\boldsymbol{B}_0(t)\cdot\boldsymbol{\sigma}/2$, Eq. (A4) is applied to solve the counter-diabatic Hamiltonian, which is in the form of $H_{\rm cd}(t) = \hbar\boldsymbol{B}_{\rm cd}(t)\cdot\boldsymbol{\sigma}/2$. In a vector representation, the counter-diabatic magnetic field is equal to a cross product,

$$\boldsymbol{B}_{\rm cd}(t) = \frac{1}{|\boldsymbol{B}_0(t)|^2}\boldsymbol{B}_0(t)\times\dot{\boldsymbol{B}}_0(t). \tag{A5}$$

Appendix B: Analytical Prediction for a Slowly-Varying Noise in the STA Process

We apply a theoretical method, similar to the approach in Ref. [30], to obtain an analytical expression for a slowly-varying classical noise in the STA process. A classical Gaussian noise $\delta H(t)$ is introduced to the total Hamiltonian, $H_{\rm tot}(t) = H_0(t) + H_{\rm cd}(t)$, during the rotation period. For convenience, the subscript 'rot' is dropped in this Appendix. Here we only consider the noise $\delta\Omega(t)$ for the drive amplitude in the $x-y$ plane. The stochastic rotating field is explicitly written as

$$\boldsymbol{B}_{\rm tot}(t) + \delta\boldsymbol{B}_\Omega(t) = ([\Omega_{\rm tot} + \delta\Omega(t)]\cos\phi(t), [\Omega_{\rm tot} + \delta\Omega(t)]\sin\phi(t), \Delta_{\rm tot}). \tag{B1}$$

The Ornstein-Uhlenbeck process is assigned for $\delta\Omega(t)$, giving $\langle\delta\Omega(t)\rangle = 0$ and $\langle\delta\Omega(t)\delta\Omega(0)\rangle = c_\Omega^2\Omega_{\rm tot}^2\exp(-\Gamma t)$ with c_Ω the reduced noise strength and Γ the noise bandwidth. We assume that $\delta\Omega(t)$ slowly varies with time (behaves similarly as a static disorder which is relevant in an adiabatic process). The fluctuated magnetic field, $\boldsymbol{B}_{\rm tot}(t) + \delta\boldsymbol{B}_\Omega(t)$, can be factorized into a fluctuated reference field, $\boldsymbol{B}_0(t) + \delta\boldsymbol{B}_0(t)$, and its counter-diabatic correction. In the spherical coordinate, the fluctuation is found from the strength, $\delta B_0(t) = |\delta\boldsymbol{B}_0(t)|$, and the

polar angle, $\delta\theta(t)$. On the first order expansion of $\delta\Omega(t)$, these two terms are given by

$$\delta B_0(t) = \sin\theta_0(\Omega_{\rm tot} \mp \omega_0 \sin\theta_0 \cos\theta_0)\frac{\delta\Omega(t)}{\Omega_{\rm tot}} + O(\delta\Omega^2(t)), \tag{B2}$$

$$\delta\theta(t) = \sin\theta_0 \cos\theta_0 \frac{\delta\Omega(t)}{\Omega_{\rm tot}} + O(\delta\Omega^2(t)). \tag{B3}$$

where the signs $\mp$ refer to the counterclockwise ($\mathcal{C}_+$) and clockwise ($\mathcal{C}_-$) directions, respectively. For the example of a single $\mathcal{C}_+$-rotation, the dynamic and Berry phase differences of $|s_\downarrow(t)\rangle$ relative to $|s_\uparrow(t)\rangle$ are fluctuated, following

$$\delta\alpha = \sin\theta_0(\Omega_{\rm tot} - \omega_0 \sin\theta_0 \cos\theta_0)\int_0^{T_{\rm rot}} \frac{\delta\Omega(\tau)}{\Omega_{\rm tot}} d\tau + O(\delta\Omega^2(t)), \tag{B4}$$

$$\delta\gamma = \omega_0 \sin^2\theta_0 \cos\theta_0 \int_0^{T_{\rm rot}} \frac{\delta\Omega(\tau)}{\Omega_{\rm tot}} d\tau + O(\delta\Omega^2(t)), \tag{B5}$$

respectively. In our experiment with a noisy pulse, we measure the total relative phase from the QST. It is however hard to directly extract γ since the noise can destroy the cancellation of the dynamic phase in the spin-echo scheme. An indirect approach is to record the input noise $\delta\Omega(t)$ and theoretically calculate the relative dynamic phase, $\alpha + \delta\alpha$, for each noisy trajectory. The corresponding relative Berry phase is estimated by $\gamma[\delta\Omega(t)] = \varphi[\delta\Omega(t)] - \alpha - \delta\alpha[\delta\Omega(t)]$, where $\varphi[\delta\Omega(t)]$ is the total relative phase. Based on the perturbed result in Eq. (B5), the statistics of the fluctuated Berry phase is characterized by the mean $\langle\delta\gamma\rangle = 0$ and the standard deviation

$$\sigma_\Omega^2 = \langle\delta\gamma^2\rangle = 8c_\Omega^2\pi^2 \sin^4\theta_0 \cos^2\theta_0 \frac{\Gamma T_{\rm rot} - 1 + \exp(-\Gamma T_{\rm rot})}{\Gamma^2 T_{\rm rot}^2}. \tag{B6}$$

A Gaussian distribution is expected for $\delta\gamma$ since the underlying noise $\delta\Omega(t)$ is Gaussian. The alternative coherence parameter, $\nu = |\langle\exp(i\gamma)\rangle|$, is fully determined by the first and second moments of $\delta\gamma$, giving

$$\begin{aligned}\nu &= \exp(-\sigma_\gamma^2/2) \\ &= \exp\left[-4c_\Omega^2\pi^2 \sin^4\theta_0 \cos^2\theta_0 \frac{\Gamma T_{\rm rot} - 1 + \exp(-\Gamma T_{\rm rot})}{\Gamma^2 T_{\rm rot}^2}\right].\end{aligned} \tag{B7}$$

Appendix C: Fidelity of a Geometric Phase Gate with the STA Protocol

The accumulated Berry phase can be utilized in the realization of geometric phase gates. In this Appendix, we numerically estimate the fidelity of a π-phase gate. In an ideal quantum operation, the quantum state is under a unitary transformation, i.e., $|\psi(t)\rangle = U|\psi(0)\rangle$.

	Protocol	$\Delta_0/2\pi$	$T_{\rm ramp}$	$T_{\rm rot}$	Fidelity
phase qubit	Adiabatic	7 MHz	350 ns	1000 ns	0.2500
($T_1 = 270$ ns, $T_2^{\rm echo} = 450$ ns)	STA	7 MHz	10 ns	30 ns	0.7023
Xmon qubit	Adiabatic	7 MHz	350 ns	1000 ns	0.8465
($T_1 = 20$ μs, $T_2^{\rm echo} = 20$ μs)	STA	7 MHz	10 ns	30 ns	0.9936

TABLE I. The fidelities of the π-phase gate in our phase qubit and a typical Xmon qubit. Both the STA and adiabatic protocols are studied. All the results are numerically obtained by the Lindbald simulation.

For the $\mathcal{C}_{+-}$ spin-echo procedure in our experiment, the unitary operator is given by $U \propto \exp[i\mathcal{S}]|0\rangle\langle 1| + \exp[-i\mathcal{S}]|1\rangle\langle 0|$. A subsequent π_x-pulse leads to the $2\mathcal{S}$-phase gate,

$$U_{\rm tot} = (-i\sigma_x)U \propto |0\rangle\langle 0| + \exp[i2\mathcal{S}]|1\rangle\langle 1|, \tag{C1}$$

where the global phase is excluded. In the special case of $\theta_0 = \arccos(3/4)$, Eq. (C1) results in a π-phase gate, i.e., $U_{\rm tot} \propto \sigma_z$.

A practical quantum operation is limited by quantum dissipation. Here we use the Lindblad equation,

$$\begin{aligned}\partial_t\rho(t) = &-\frac{i}{\hbar}[H(t),\rho(t)] + \frac{1}{T_1}\left[\sigma_-\rho(t)\sigma_+ - \frac{1}{2}\sigma_+\sigma_-\rho(t) - \frac{1}{2}\rho(t)\sigma_+\sigma_-\right] \\ &+\frac{2}{T_2^{\rm echo}}\left[\sigma_+\sigma_-\rho(t)\sigma_+\sigma_- - \frac{1}{2}\sigma_+\sigma_-\sigma_+\sigma_-\rho(t) - \frac{1}{2}\rho(t)\sigma_+\sigma_-\sigma_+\sigma_-\right],\end{aligned} \tag{C2}$$

to numerically estimate the time evolution of the density matrix $\rho(t)$, where $\sigma_+ = |1\rangle\langle 0|$ and $\sigma_- = |0\rangle\langle 1|$ are two Lindblad operators. A quantum dynamical map is then defined between the initial and final density matrices ($\rho(0)$ and $\rho(t_{\rm f})$ respectively), i.e., $\rho(t_{\rm f}) = \sum_{i,j=1}^{4}\chi_{i,j}u_i\rho(0)u_j^\dagger$, where the four operators of the SU(2) group, $\{u_1 = I, u_2 = \sigma_x, u_3 = \sigma_y, u_4 = \sigma_z\}$, are used as the expansion bases. The 4×4 χ-matrix independent of the initial density matrix $\rho(0)$. For an ideal π-phase gate, the χ-matrix satisfies $\chi_{i,j}^{\rm ideal} = \delta_{i,4}\delta_{j,4}$. The accuracy of a practical π-phase gate can be characterized by its gate fidelity, given by [9]

$$F = {\rm Tr}\left\{\chi^{\rm ideal}\chi\right\}. \tag{C3}$$

In Table I, we provide the numerical estimations of F for our phase qubit ($T_1 = 270$ ns and $T_2^{\rm echo} = 450$ ns) and a typical Xmon qubit ($T_1 = 20$ μs and $T_2^{\rm echo} = 20$ μs). Both the STA ($T_{\rm ramp} = 10$ ns and $T_{\rm rot} = 30$ ns) and adiabatic ($T_{\rm ramp} = 350$ ns and $T_{\rm rot} = 1000$ ns) protocols

are considered. Our numerical results show that the STA protocol can help establish a higher fidelity in an operation time much shorter than that required by the adiabatic theorem. It will be interesting to explore the STA protocol in the Xmon qubit (e.g., the STA π-phase gate with fidelity $> 99\%$) in the future.

---

[1] M. V. Berry, Proc. R. Soc. London Ser. A **392**, 45 (1984).

[2] R. Y. Chiao and Y.-S. Wu, Phys. Rev. Lett. **57**, 933 (1986).

[3] T. Bitter and D. Dubbers, Phys. Rev. Lett. **59**, 251 (1987).

[4] A. Shapere and F. Wilczek, *Geometric Phases in Physics* (World Scientific, Singapore, 1989)

[5] D. Xiao, M.-C. Chang and Q. Niu, Rev. Mod. Phys. **82**, 1959 (2010).

[6] E. Sjöqvist, Physics **1**, 35 (2008).

[7] J. A. Jones, V. Vedral, A. Ekert, and G. Castagnoli, Nature (London) **403**, 869 (2000).

[8] D. Leibfried, *et al.*, Nature (London) **422**, 412 (2003).

[9] A. Abdumalikov Jr, *et al.*, Nature (London) **496**, 482 (2013).

[10] H. Wu, *et al.*, Phys. Rev. A **87**, 032326 (2013).

[11] J. Kelly, *et al.*, Nature (London) **519**, 66 (2015).

[12] M. Demirplak and S. A. Rice, J. Phys. Chem. A **107**, 9937 (2003).

[13] M. Berry, J. Phys. A: Math. Theor. **42**, 365303 (2009).

[14] X. Chen, I. Lizuain, A. Ruschhaupt, D. Guéry-Odelin, and J. G. Muga, Phys. Rev. Lett. **105**, 123003 (2010).

[15] S. Masuda and K. Nakamura, Proc. R. Soc. A **466**, 1135 (2010).

[16] E. Torrontegui, *et al.*, Adv. At. Mol. Opt. Phys **62**, 117 (2013).

[17] B. T. Torosov, S. Guérin, and N. V. Vitanov, Phys. Rev. Lett. **106**, 233001 (2011).

[18] J. M. Martinis and M. R. Geller, Phys. Rev. A **90**, 022307 (2014).

[19] Y. Aharonov and J. Anandan, Phys. Rev. Lett. **58**, 1593 (1987).

[20] S.-L. Zhu and Z. D. Wang, Phys. Rev. Lett. **89**, 097902 (2002).

[21] M. G. Bason, *et al.*, Nat. Phys. **8**, 147 (2012).

[22] J. Zhang, *et al.*, Phys. Rev. Lett. **110**, 240501 (2013).

[23] J. M. Martinis, Quantum Inf. Process. **8**, 81 (2009).

[24] E. Lucero, *et al.*, Nat. Phys. **8**, 719 (2012).

[25] M. Möttönen, J. J. Vartiainen, and J. P. Pekola, Phys. Rev. Lett. **100**, 177201 (2008).

[26] P. Leek, *et al.*, Science **318**, 1889 (2007).

[27] S. Berger, *et al.*, Phys. Rev. A **87**, 060303 (2013).

[28] S. Filipp, *et al.*, Phys. Rev. Lett. **102**, 030404 (2009).

[29] S. Berger, *et al.*, Phys. Rev. B **85**, 220502 (2012).

[30] G. De Chiara and G. M. Palma, Phys. Rev. Lett. **91**, 090404 (2003).

[31] D. M. Tong, E. Sjöqvist, L. C. Kwek, and C. H. Oh, Phys. Rev. Lett. **93**, 080405 (2004).

[32] J. Du, L. Hu, Y. Wang, J. Wu, M. Zhao, and D. Suter, Phys. Rev. Lett. **101**, 060403 (2008).